Interlayer vacancy defects in AA-stacked bilayer graphene: Density functional theory predictions

A. Vuong[1], T. Trevethan[1], C. D. Latham[2], C. P. Ewels[3], D. Erbahar[3,4], P. R. Briddon[5], M. J. Rayson[5], M. I. Heggie[2]

[1]Department of Chemistry, Faculty of Engineering and Physical Sciences, University of Surrey, Guildford, GU2 7XH, United Kingdom
[2] Department of Chemistry, Loughborough University, Loughborough, Leicestershire, LE11 3TU
[3] Institut des Materiaux Jean Rouxel (IMN), Universite de Nantes, Centre national de la recherche scientifique (CNRS), 2 rue de la Houssiniere, BP32229, 44322 Nantes, France
[4] Physics Department, Gebze Technical University, 41400 Kocaeli, Turkey
[5] School of Electrical and Electronic Engineering, Newcastle University, Newcastle upon Tyne, NE1 7RU, United Kingdom

Abstract. AA-stacked graphite and closely related structures, where carbon atoms are located in registry in adjacent graphene layers, are a feature of graphitic systems including twisted and folded bilayer graphene, and turbostratic graphite. We present the results of *ab initio* density functional theory calculations performed to investigate the complexes that are formed from the binding of vacancy defects across neighbouring layers in AA-stacked bilayers. As with AB stacking, the carbon atoms surrounding lattice vacancies can form interlayer structures with sp^2 bonding that are lower in energy than in-plane reconstructions. The sp^2 interlayer bonding of adjacent multivacancy defects in registry creates a type of stable sp^2 bonded 'wormhole' or tunnel defect between the layers. We also identify a new class of 'mezzanine' structure characterised by sp^3 interlayer bonding, resembling a prismatic vacancy loop. The V_6 hexavacancy variant, where six sp^3 carbon atoms sit midway between two carbon layers and bond to both, is substantially more stable than any other vacancy aggregate in AA-stacked layers. Our focus is on vacancy generation and aggregation in the absence of extreme temperatures or intense beams.

1. Introduction

Interlayer interaction in multilayered graphene, graphite and other carbon nanostructures such as multiwalled nanotubes and carbon onions, plays an important role in their mechanical and electrical properties [1]. The interlayer binding in these systems is much weaker than the covalent sp^2 carbon-carbon bonding within the layers and it is this feature that leads to their highly anisotropic behaviour [2]. However, the presence of intrinsic defects that result in the formation of covalent bonds across adjacent layers can drastically alter the material properties [3]. Intrinsic defects created by atomic displacements, lattice vacancies and interstitials, can be introduced to graphitic systems under energetic particle irradiation, and this can be used to control and modify the structure and properties of these materials.

The self-interstitial and lattice vacancy represent the two most fundamental intrinsic defects in graphite, and as such, are widely studied. In multilayered graphitic systems the lowest energy configuration for an isolated self-interstitial, known as a spiro-interstitial, lies at the midpoint between adjacent layers and forms two covalent sp^3-hybridised bonds to each layer, pinning them together [3–5]. However very stable interlayer bonds can also be

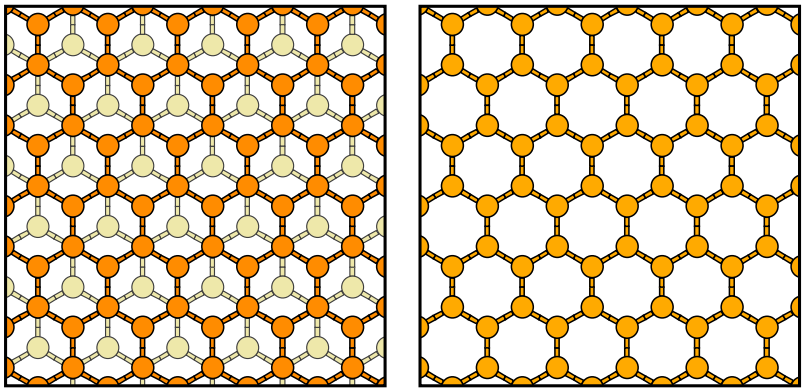

(a) (b)

Figure 1. Schematic of bilayer graphene with dark-coloured atoms as top layer and pale-coloured atoms as bottom layer for (a) AB stacked and (b) AA stacked.

formed from interaction between the under coordinated atoms surrounding vacancy defects in neighbouring layers. These interlayer divacancy complexes have very low activation energies to form (typically 0.2–0.3 eV) [6, 7], and combined with the modest activation energy for monovacancy diffusion in graphene ($\sim$ 1.2 eV) [8], are expected to play an important role in the response of a multilayered system to displacing irradiation. In addition to pairs of monovacancies bonding between the layers, the aggregation of additional diffusing vacancies can result in the formation of extended interlayer defects, such as the 'ramp' defect, which comprises a ribbon of graphene connecting adjacent layers [7]. *Ab initio* modelling shows that such defects should form and they have been directly observed in transmission electron microscopy images of irradiated graphite [7].

The lowest energy configuration of crystalline graphite and multilayered graphene is the Bernal structure [2] or AB stacking (Fig. 1(a)), which has a spacing between the layers of approximately 335 pm. This is by far the most common structure observed experimentally. However, owing to the relatively low strength of interlayer forces, the energetic cost of relative translation of the layers, or basal slip, is quite small. This often leads to significant regions of alternate stacking arrangements, most commonly rhombohedral or ABC stacking [9] and AA stacking. ABC stacking is where the carbon atoms in the fourth layer are located directly in registry with the first layer and the third layer is shifted with respect to the first and second layer. AA stacking is where the carbon atoms in each layer are located directly in registry (Fig. 1(b)). It is the highest energy stacking configuration, and represents a maximum on the gamma surface [10]. AA stacking has not been observed in bulk graphite; however, localised regions have been observed in many graphitic-like systems. For example, superlattices of domains close to AA stacking are formed in the Moiré patterns seen in scanning electron microscope images of rotated planes of bilayer graphene and in twist grain boundaries in graphite [11]. Recently, pure AA-stacked graphite has been produced on diamond surfaces [12] and AA stacking is also found to occur at folds of monolayer [13] and bilayer graphene [14]. Since AA stacked regions then play a significant role in many graphitic and nanostructured carbon systems, it is important to understand the nature of interlayer defects within this structure: the structures that are formed, their energetics and how they will change the material properties.

In this work, we employ *ab initio* density functional theory (DFT) calculations to investigate the formation of interlayer vacancy complexes in AA-stacked regions. These

demonstrate how the behaviour of populations of vacancies is dramatically different to that in AB stacked regions. In addition, to considering interlayer vacancy dimers, we also investigate the formation of larger vacancy aggregates from a stepwise addition of mobile single vacancies arriving in pairs in adjacent layers. We find two different morphologies of extended vacancy defect: 'wormhole' or 'tunnel' structures [15, 16] characterised by sp^2 bonding and 'mezzanine' or 'mid-layer' structures characterised by sp^3 bonding. We compare the formation energies of these extended defects with purely coplanar aggregates to show how they are energetically favoured over the most stable in-plane complexes.

We note that our use of sp^2 and sp^3 nomenclature indicates the number of carbon neighbours (3 and 4 respectively), and a degree of double-bond character in the case of sp^2, as demonstrated by the relatively short C-C bonds. In practice due to the local curvature, such sp^2 bonds will have a degree of sp^3 character.

2. Method

To investigate the formation of interlayer bonding between vacancy defects in a bilayer graphene structure with both good accuracy and computational efficiency, we employ the density functional theory (DFT) method implemented in the AIMPRO simulation package [17–20]. Valence electrons are described by a $pdpp$ basis set possessing 22 independent Gaussian-based functions, where both the spin polarised local density approximation (LDA) [21], and the PBE96 generalised gradient approximation (GGA) [22] are used for the exchange-correlation functional. Norm-conserving pseudo-potentials are used to represent core electrons [23]. Other details of this method and its applicability to graphitic systems has been the subject of earlier work [8, 24]. The numerical integration over the Brillouin zone is performed using the Monkhorst-Pack scheme [25] and the size of the $\boldsymbol{k}$-point mesh is $4\times4\times2$. The states are occupied according to the first-order Methfessel-Paxton scheme [26] with $k_{\mathrm{B}} = 0.01$ eV.

Neither the LDA nor PBE functionals correctly describe London dispersion interactions, which are a component of the interlayer binding in perfect graphite. Nevertheless, there is also a significant component of interlayer binding arising from orbital overlap, and overall the LDA does reproduce the interlayer interaction energy and interlayer separation quite well [27–29], whereas the GGA predicts nearly no interlayer binding. Possible reasons for this behaviour are discussed in the work previously cited in [8]. Although the GGA functional does not bind the layers, it does correctly reproduce relative stacking energies with interlayer spacing from LDA calculations. For interlayer spacing constrained at the LDA value, we find that relative energy changes are usually insensitive to the exchange correlation functional employed, which suggests that the results are not significantly affected by the omission of London dispersion forces.

The defects are constructed in a $6a\times3b\times\frac{3}{2}c$ orthorhombic supercell, with $b = a\sqrt{3}$, based on a 144-atom graphene bilayer, when no defect is present. The optimised interlayer separation, $c/2$, given by the $pdpp$ basis set and the LDA for both AB stacking (325 pm) and AA stacking (352 pm) in the present work is not significantly different from that found by earlier calculations [28, 29], given that the basis sets and parameterization of the exchange-correlation functional are not identical. Thus, this geometry has an empty gap of size c separating the model structure from its images in the neighbouring supercells.

In the following sections the LDA values are given, followed by the GGA values in parentheses, both using the LDA optimized cell parameters for the perfect bilayer.

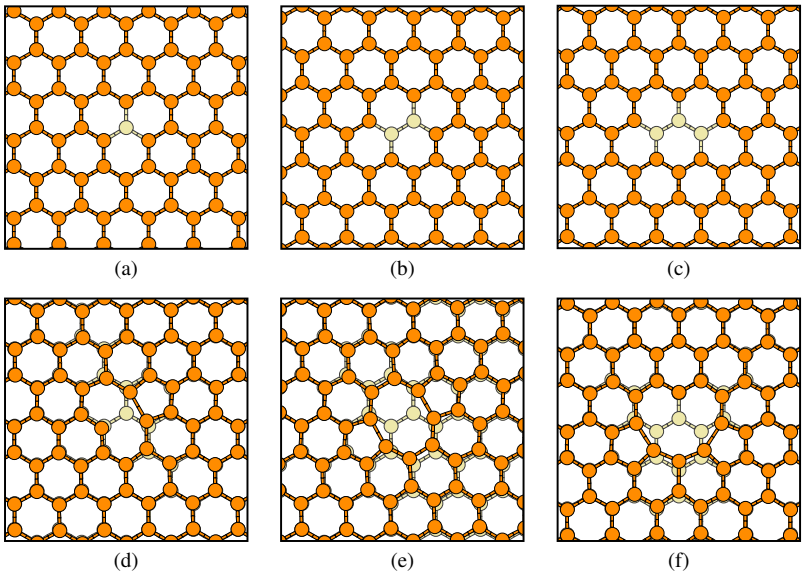

Figure 2. Model vacancy structures in bilayer graphene viewed along the prismatic direction where the atoms in the nearer layer are shown in a darker shade than those behind. Unoptimised models for (a) monovacancy, (b) divacancy and (c) trivacancy. Optimised structures for (d) monovacancy, (e), divacancy and (f) trivacancy.

3. Results

An isolated monovacancy, formed by the removal of a single carbon atom from the graphene lattice, is susceptible to a Jahn-Teller distortion [30, 31] which results in the formation of a bond about 180–190 pm long between two of the three under-coordinated atoms [8, 32]. The formation energy of this defect is estimated to be about 7.9 eV LDA (7.4 eV GGA) [8]. The predicted activation barrier for migration of a monovacancy within the graphite layer is found to be $E_a \approx 1.2$ eV by Latham *et al.* [8]; however, Wadey *et al.* recently found a lower activation barrier in buckled graphene with a fourfold coordinated structure for the transition state [33].

3.1. Interlayer divacancy and tetravacancy

When two migrating vacancies meet within the same graphene sheet, they can coalesce to form the very stable and immobile nearest neighbour 5-8-5 divacancy structure (Fig. 2(e)) [8, 34–36] which is remarkably stable: its energy is about 7.9 eV (7.0 eV) lower than two separated monovacancies, making its formation energy approximately equal to that for a single monovacancy. However, if two vacancies in adjacent layers come into registry with each other, one or more of the under coordinated atoms surrounding each vacancy can form bonds across the interlayer gap [3]. In AB-stacked graphite, DFT calculations have shown that there are four different forms of these energetically bound cross-layer divacancy structures [8].

In the case of AA stacking, there is only one configuration, which results in stable interlayer bonding. This has one vacancy directly above the other and all the surrounding under coordinated atoms in registry (Fig. 2(a)). In this registry there are two likely bonding configurations: the first has only one interlayer bond (Fig. 3(a), (d)) while the second makes three bonds between all six under-coordinated atoms. The more stable configuration with one

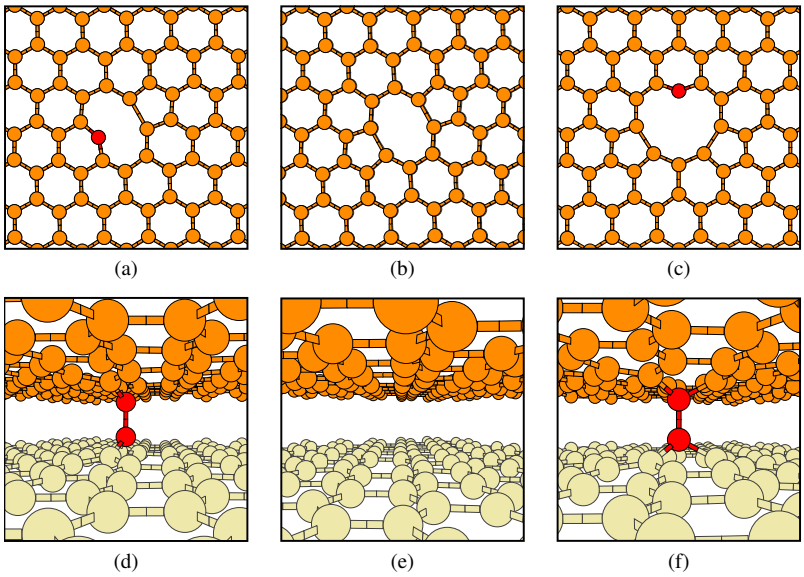

Figure 3. Geometry optimised AA-stacked bilayer graphene complexes of in plane view (a) divacancy species V_1-V_1 with one sp^2 interlayer bond, (b) tetravacancy species, V_2(5-8-5)-V_2(5-8-5) (no interlayer sp^2 bonds), (c) hexavacancy species V_3-V_3 with one sp^2 interlayer bond and its out of plane view in (d), (e) and (f). The red atom has an sp^2 interlayer bond to its counterpart in the neighbouring graphene sheet.

interlayer bond has a total energy 2.8 eV (2.4 eV) lower than two isolated monovacancies, while the configuration with three interlayer bonds is only 2.5 eV (2.0 eV) more stable than isolated monovacancies. The single-bond configuration has coplanar reconstruction within each of the two graphene sheets, similar to the pentagonal motif of the monovacancy. These are replaced in the three-bond configuration by three closely packed interlayer bonds. These bonds are highly strained and distorted, which suggests why the energy of this structure energy is higher than the first form.

Migration of additional monovacancies to this structure can result in larger multivacancy complexes. We first consider the addition of one vacancy in each layer, leading to a pair of coplanar divacancies in registry (Fig. 3(b), (e)). This leads to V_2-V_2 which is more stable than an alternative tetravacancy V_1-V_3 by 0.9 eV (0.9 eV) per vacancy. To make four interlayer bonds between two of these divacancy species, the in plane reconstructions forming the fivefold rings must be broken, which costs energy. However, even in this case the resultant species is almost energetically neutral: it is about 0.4 eV more stable for interlayer binding using the LDA, and 0.9 eV less stable using the GGA than the two in-plane divacancies.

The energy of the system can be lowered by an additional 1.1 eV (1.0 eV) per layer by rearranging the nearest neighbour V_2(5-8-5) defect that is directly above the other V_2(5-8-5) defect into three pentagons and three heptagons V_2(555-777) haeckelite structure divacancy with a Stone-Wales type bond rotation [34]. The V_2(555-777) that is directly above the other V_2(555-777) can be transformed into V_2(5555-6-7777) with a Stone-Wales bond rotation [34]. The V_2(5555-6-7777) formation energy of 3.6 eV (3.1 eV) per vacancy is found to be between 4.0 eV (3.5 eV) for V_2(5-8-5) and 3.4 eV (3.0 eV) for V_2(5555-6-7777), which is in good agreement with other studies [53]. However, to reach this state relatively large barriers (~5 eV according to DFT calculations [8]) must be crossed, which are thermally inaccessible except

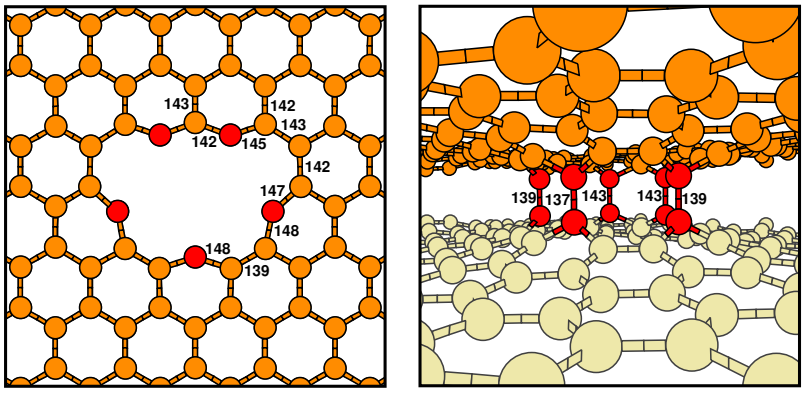

(a) (b)

Figure 4. Geometry optimised structure of V_3-V_3 wormhole defect structure: (a) view along the prismatic axis (b) view along the basal plane. Bond lengths marked in picometres.

at very high temperatures (above ~1900 K making usual assumptions of attempt frequency, $\sim 10^{13}$Hz, and zero entropy of activation)

3.2. Interlayer hexavacancy: Wormhole and mezzanine structures

In the case of two trivacancies in registry in adjacent layers, which are formed from the addition of another migrating monovacancy in each layer (Fig. 2(c)), there are again a number of different possible configurations. A single co-planar trivacancy reconstructs to form a pair of five-membered rings and a single dangling bond (Fig. 2(f)). An alternative trivacancy can consist of a monovacancy in one layer and an in-plane divacancy in another. The V_1-V_2 is more stable than the V_3(5-10-5) by 1.5 eV (1.5 eV) per vacancy. When two trivacancies V_3-V_3 are in registry, a single sp^2 bond forms between the two dangling bonds releasing 2.0 eV (1.1 eV) (Fig. 3(c) and (f)). This is analogous to the interlayer bonding for the two monovacancies discussed above, with the same calculated energy release.

However, in this case the reconstructed bonds, which form the five-membered rings, these are more widely spaced, and it becomes energetically favourable to break these and form additional interlayer bonds. Indeed, the formation of five interlayer bonds (by breaking the two five-membered rings in each layer) releases 4.8 eV (3.1 eV) in total (Fig. 4). This defect is more stable, by 0.9 eV (0.1 eV) than a purely in-plane V_6 loop (a structure corresponding to a hexagonal ring of carbon atoms removed from the lattice) making it the most stable V_6 species proposed in graphite to date [37, 38].

This type of reconstruction, with complete sp^2 bonding around multivacancies in adjacent layers, creates a pore in the bilayer. The chemical nature of this will be fundamentally different to holes or pores in monolayers, whose edges are unsaturated, dangling bonds. These sp^2-bonded pores resemble the wormholes predicted by Margine *et al* [16]. Their wormholes arise from the rearrangement of atoms, leading to pentagons, and require an increased interlayer separation [16]. In our case the structural defect is characterised by a sequential aggregation of vacancies, and does not require a substantially increased interlayer separation to form.

However, the most stable structure for six vacancies in AA-stacked systems is not the wormhole, but another type of morphology, hereafter called a ‘mezzanine defect’. This is constructed by removing a hexagonal ring of six atoms from one sheet, then translating a ring

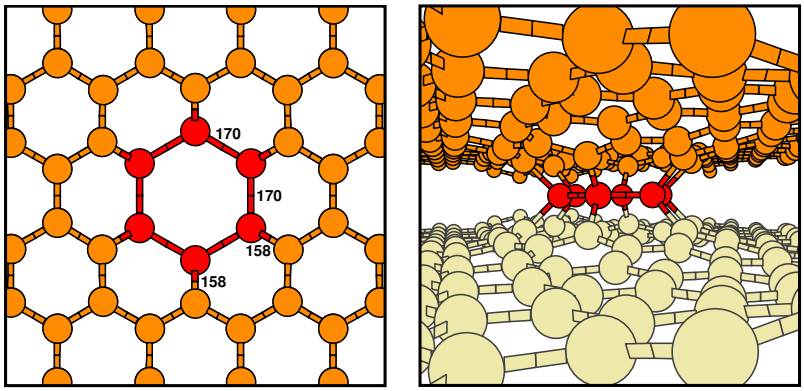

(a) (b)

Figure 5. Geometry optimised structure of V_3-V_3 mezzanine defect structure: (a) view along the prismatic axis (b) view along the basal plane. Bond lengths marked in picometres.

of six atoms from an adjacent sheet neighbouring the hexavacancy by half of the interlayer separation, and allowing the ring to expand so that it forms a symmetrical arrangement of fourfold-coordinated bonds with both nearest neighbouring graphene sheets (Fig. 5). Thus, the hexavacancy is shared or split between two neighbouring graphene sheets. Its structure is characterised by a six fold ring of sp^3-bonded carbon atoms with a bond length within the ring of 158 pm, located midway between the two layers (a 'mezzanine'). This bonding arrangement resembles the AA-stacked zigzag prismatic edge dislocation found by Suarez-Martinez *et al* [39]. The formation energy per vacancy for the mezzanine defect is calculated to be only 2.9 eV (2.9 eV). Hence, the split-hexavacancy, or mezzanine defect, has lower total energy than the alternative V_3-V_3 wormhole by 0.8 eV (0.2 eV). The mezzanine is also more favourable in energy compared with coplanar V_6 armchair and zigzag vacancy lines by 2.1 eV (0.3 eV) and 3.7 eV (1.5 eV), respectively. Two pentagones are formed at both ends of the chain of the coplanar V_6 armchair and zigzag vacancy lines, similar to the dislocation defect by Jeong *et al.* [40]. The mezzanine is 1.6 eV (0.2 eV) more stable than a V_6 loop, where the hexavacancy ring occupies a single layer only, without interlayer bonding. Moreover, the energy per vacancy for the mezzanine defect is significantly smaller than for the nearest neighbour V_2 defect, which costs E_f = 3.9 eV (3.5 eV) per vacancy, and substantially less than isolated V_1, where E_f = 7.9 eV (7.4 eV).

The energetics of the various structures of co-planar and interlayer vacancy complexes up to V_6 are listed in Table 1 for both the LDA and GGA functionals. Here, the total formation energy is defined relative the perfect (AA-stacked) lattice. The binding energy of an interlayer defect is defined as the energy released from the interlayer binding of the isolated defects in each layer. Where there is no label this implies no covalent interlayer bonding. The label 'wormhole' means all under coordinated atoms in each layer bind to form interlayer bonds, while 'mezzanine' refers to the interlayer sp^3 coordinated layer formation.

For the monovacancy in registry with another in an adjacent layer (V_1-V_1), there is a small positive interaction energy ($\sim$ 0.1 eV) without the formation of any interlayer sp^2 bonds. The formation of a single interlayer bond (by crossing a 0.3 eV barrier) releases a further $\sim$ 3 eV. As described above, the formation of further interlayer bonds costs more energy in breaking the reconstructions than is gained from the new bonds. In the case of the co-planar divacancy, two in adjacent layers in registry (V_2(5-8-5) V_2(5-8-5)) interact very weakly (0.06 eV (0.03 eV)). However, when the reconstructions are broken and the under coordinated

Table 1. Calculated formation energies, formation energies per vacancy, and interlayer binding energies in eV for different vacancy complexes in AA-stacked bilayer graphene using LDA and GGA functionals. Formation energies E_f are with respect to the perfect AA-stacked structure; interlayer binding energies E_b are with respect to the energies of equivalent isolated monolayer vacancy complexes in AA-stacked bilayer graphene. The notation V_n-V_m implies n vacancies in top layer, and m in the bottom layer. The most stable V_x species are given in bold.

Structure	Interlayer bonds	LDA			GGA		
		E_f	E_f/V	E_b	E_f	E_f/V	E_b
V_1 (Fig. 2(d))		**7.94**	**7.94**		**7.41**	**7.41**	
V_1-V_1		15.76	7.88	0.13	14.72	7.36	0.11
V_1-V_1 (Fig. 3(a), (d))	1 sp^2	**13.11**	**6.56**	2.78	**12.41**	**6.20**	2.42
V_1-V_1 wormhole	3 sp^2	13.35	6.68	2.54	12.88	6.44	1.95
V_2		**7.87**	**3.94**		**6.99**	**3.49**	
V_2-V_2 wormhole	4 sp^2	15.32	3.83	0.42	14.89	3.72	−0.92
V_2(5-8-5) V_2(5-8-5) (Fig. 3(b), (e))		15.80	3.95	−0.06	14.00	3.50	−0.03
V_2(555-777) V_2(555-777)		**13.51**	**3.38**	**2.23**	**11.93**	**2.98**	**2.04**
V_2(5555-6-7777) V_2(5555-6-7777)		14.21	3.55	1.53	12.39	3.10	1.59
V_3 (Fig. 2(f))		**11.54**	**3.85**		**10.20**	**3.40**	
V_1-V_2		16.13	5.38	−0.32	14.72	4.91	−0.32
V_1-V_3		19.39	4.85	0.24	17.46	4.37	0.24
V_2-V_3		19.74	3.95	−0.32	17.46	3.49	−0.27
V_6 mezzanine (Fig. 5)	6 sp^3	**17.53**	**2.92**	5.56	**17.15**	**2.86**	3.26
V_3-V_3 wormhole (Fig. 4)	5 sp^2	18.28	3.05	4.81	17.34	2.89	3.07
V_6 loop		19.13	3.19	3.96	17.32	2.89	3.09
V_6 armchair line		19.63	3.27	3.46	17.45	2.91	2.96
V_3-V_3 (Fig. 3(c), (f))	1 sp^2	21.05	3.51	2.04	19.27	3.21	1.14
V_6 zigzag line		21.23	3.54	1.86	18.64	3.11	1.77

atoms form four bonds across the interlayer gap 0.4 eV (0.9 eV) is released. The contrast between this behaviour and that of the monovacancy shows that there is a very fine balance of energies in determining whether it is energetically favourable to form an interlayer bond, relating to the stability of in-plane reconstructions and the strained bonding configurations that are involved in the formation of sp^2 bonds across the interlayer gap. We note that there is an alternative V_4 structure consisting of an in-plane V_3 and a single vacancy, however this is 3.6 eV (3.5 eV) less stable than the ground-state V_2-V_2 (5-8-5) species considered above. In the case of the V_3-V_3 complexes (V_6 in total) the table shows a progression of bonding energies from one interlayer bond to five interlayer bonds to the mezzanine structure. The formation energies of co-planar V_6 complexes (in a single layer) are shown for comparison.

4. Magnetism

Any study of graphitic materials should always be alert to the possibility that defect structures may possess a net magnetic moment [5]. In some instances this might be due to the presence sp^3-hybridized carbon atoms [43, 44]. Also, it is well-established that vacancies in graphite are magnetic [8, 46]. Moreover, according to Lieb's theorem [52], ferromagnetism can arise in the delocalized π-system of graphene sheets when the presence of point defects causes an imbalance in electronic band structure of the bipartite sublattice. In our investigation V_1, V_1-V_1 and V_3 appear to have one partially-occupied sp^2-orbital per plane, which contribute to a non-zero magnetic moment. For V_1 the net magnetic moment is calculated to be

Table 2. Calculated magnetic moments of the model systems. The notation V_n-V_m represents a defect with n vacancies in the top layer, and m in the bottom layer.

Structure	Interlayer bonds	μ (μ_B)	
		LDA	GGA
V_1 (Fig. 2(d))		~ 1.0	1.5
V_1-V_1		2.5	~ 1.0
V_1-V_1 wormhole	3 sp^2	0.0	0.5
V_3 (Fig. 2(f))		1.1	1.0
V_1-V_2		1.0	1.0
V_2-V_3		1.0	1.3
V_1-V_3		1.5	2.0
V_6 loop		2.0	~ 3.0
V_6 armchair line		~ 2.0	~ 2.0

about 1.0–1.5 μ_B, in good agreement with earlier work [5, 45, 47–49]. Similarly, we predict that the magnetic moment for V_3 to be about 1.0 μ_B, which is again close to earlier estimates [45, 47, 51]. Structural defects that are composed of V_1 or V_3 in one of the layers possess a magnetic moment as seen for V_1-V_2, V_1-V_3 and V_2-V_3. The divacancy wormhole, V_1-V_1 might possess a non zero magnetic moment. Structures without dangling bonds possess a zero magnetic moment. Mulliken population analysis of the defect shows that it has an unpaired electron within a p_z-orbital. In the case of the V_6 loop, conflicting results are found for the net magnetic moment: it is zero, but with antiferromagnetic ordering in [45] and non-zero (6.00 μ_B) in [47]. The V_6 zigzag line possesses a zero magnetic moment and V_6 armchair line possesses a non zero magnetic moment. These are in agreement with published results; however, the armchair line can possess metallic and semi-conducting behaviour, which is dependent on the width [50].

5. Discussion

Calculations employing DFT have been used in the present work to investigate the aggregation of vacancies in AA-stacked bilayer graphene. The results show that mobile single vacancies in adjacent layers can combine to form structures composed entirely of threefold-coordinated atoms with cross-layer bonds, and that they are more stable than the corresponding forms of vacancy complexes possessing only coplanar reconstruction (i.e. pentagon and octagon rings). Thus, we have identified the most stable V_n species in AA-stacked graphite for n = 1–6.

It is clear from these simulations that the mezzanine defect is the lowest energy structure for the hexavacancy (V_6) in AA-stacked regions of bilayer graphene. Although the GGA result places the mezzanine defect and wormhole very close in energy, this may well be an artefact of the functional, which yields almost no interlayer interaction, instead of giving a weak physical attraction between the graphene layers. The mezzanine defect, more than the wormhole, is penalised by its requirement to span the interlayer space with two single bonds and a distorted tetrahedral bond angle, and the GGA will tend to produce an artificial instability.

Furthermore, when viewed from the point of view of dislocation theory, each of the non-linear defects is a prismatic vacancy dislocation loop. The dislocation loop for the mezzanine defect has Burgers vector $\mathbf{c}/2$, i.e. a partial dislocation, whereas for the wormhole it is $\mathbf{c}$, i.e. a perfect dislocation. Elastic energies vary with the square of the Burgers vector, thus favouring the mezzanine defect, notwithstanding its increased radius compared with the wormhole.

The $\mathbf{c}/2$ loop dislocation is of the same nature as the prismatic dislocations discussed

by [39], except its curvature means it alternates between zigzag and armchair character around the structure. In this regard, it should be noted that [39] gave the armchair core as disconnected from any other layer; however, in this work it is connected via fourfold-coordinated carbon atoms in the same way as the zigzag core.

6. Conclusion

The process of vacancy aggregation can lead to curious structural defects, and not always the most thermodynamically stable arrangements are produced. In the case of the ground state (AB) stacking of the bilayer, the outcome of vacancy aggregation is found to be a combination of lines, prismatic loops and ramps [7]. However, there are situations where bilayer stacking is perturbed to approach AA stacking, in the limiting case of pure AA stacking, where it is found in the present work that low-energy cross-layer vacancy complexes possibly exist that are just as remarkable as those in normal AB graphite.

Even though the nearest-neighbour divacancy is a rather deep local energy minimum, it can dimerize across the interlayer space with four interlayer bonds. This binding across the graphene layers is very similar to that seen in AB-stacked bilayers, and is not inhibited by the larger interlayer separation of AA-stacked bilayer graphene.

Two new classes of structure are identified for hexavacancies. The first is a V_6 wormhole comprising a continuously bonded network of threefold-coordinated carbon atoms. It is expected that these pore-like structures could grow in size for larger vacancy aggregates, and are likely to exhibit unique chemical properties compared with the widely studied pores in monolayer graphene, where the pore edges are typically hydrogenated or contain dangling bonds. For larger holes these will be able to open further, closer resembling folded graphene edges. It is quite possible that such wormhole pore structures can be used as for diffusive transport of molecules such as nitrogen and water [41].

The second class is mezzanine defects, where a split vacancy loop forms a structure bounded by a ring of fourfold-coordinated carbon atoms, with bonds that span the space between adjacent graphene sheets. It is notable that the mezzanine defect is the lowest energy state for a system of six vacancies in AA-stacked bilayer graphene, and has by far the lowest formation energy per vacancy of all the systems we have studied.

The hexavacancy is already known to be a key defect structure in heavily irradiated graphite. Early positron-annihilation experiments identified V_6 species as a major and abundant species after heavy neutron irradiation, stable up to 1773 K [37]. The assignment was based on positron lifetime for the stable species of 350 ps, which corresponded to calculated lifetime for a stable C_{6v}-symmetry in-plane V_6 ring. Similarly implantation of ETU10-grade graphite with 350-keV C^+ ions were characterised by positron annihilation doppler broadening, and stable species tentatively ascribed to V_6 were observed up to 1773 K [38]. It is possible that the mezzanine structure for V_6 described here could also be responsible for these positron annihilation observations, since both species should be expected to have similar positron lifetimes. The smallest cavity dimension determines the positron lifetime associated with that cavity: for the mezzanine V_6 it is the interlayer space of 0.50 nm, whereas for an in-plane V_6 loop it is the diameter of the missing C_6 hexagon, 0.57 nm.

Careful control of temperature and nature of radiation damage could provide viable routes to new and complex nanostructures. In detail, the relative proportion of each nanostructure will be dependent on the kinetics and sequence of approach of the vacancies, which can depend on the local strain field [42] and require further investigation.

Acknowledgments

A. Vuong thanks University of Surrey for her studentship, A. Vuong, M. I. Heggie and C. D. Latham thank EDF Energy Generation Ltd for financial support. T. Trevethan thanks Innovate UK project The influence of graphite irradiation creep on plant life optimisation (24792-167222) for financial support. The views expressed are those of the authors and not necessarily those of the sponsors.

References

[1] Choi W, Lahiri I, Seelaboyina R and Kang Y S 2010 *Crit. Rev. Solid State Mater. Sci.* **35** 52–71
[2] Bernal J D 1924 *Proc. R. Soc. Lond., Ser.* A **106** 749–773
[3] Telling R H, Ewels C P, El-Barbary A A and Heggie M I 2003 *Nature Mater.* **2** 333–337
[4] Heggie M I, Eggen B R, Ewels C P, Leary P, Ali S, Jungnickel G, Jones R and Briddon P R 1998 *Fullerenes: Chemistry, Physics, and New Directions* (*Recent Advances in the Chemistry and Physics of Fullerenes and Related Materials* vol 6) ed Kadish K M and Ruoff R S (Pennington, NJ: The Electrochemical Society) pp 60–67
[5] Latham C D, Heggie M I, Gámez J A, Suárez-Martínez I, Ewels C P and Briddon P R 2008 *J. Phys: Condens. Matter.* **20** 395220
[6] Trevethan T, Latham C D, Heggie M I, Rayson M J and Briddon P R 2014 *Phys. Rev.* B **90** 174108
[7] Trevethan T, Dyulgerova P, Latham C D, Heggie M I, Seabourne C R, Scott A J, Briddon P R and Rayson M J 2013 *Phys. Rev. Lett.* **111** 095501
[8] Latham C D, Heggie M I, Alatalo M, Öberg S and Briddon P R 2013 *J. Phys: Condens. Matter.* **25** 135403
[9] Amelinckx S and Delavignette P 1960 *J. Appl. Phys.* **31** 2126–2135
[10] Telling R H and Heggie M I 2003 *Philos. Mag. Lett.* **83** 411–421
[11] Li G, Luican A, Lopes Dos Santos J M B, Castro Neto A H, Reina A, Kong J and Andrei E Y 2010 *Nature Phys.* **6** 109–113
[12] Lee J K, Lee S C, Ahn J P, Kim S C, Wilson J I B and John P 2008 *J. Chem. Phys.* **129** 234709
[13] Liu Z, Suenaga K, Harris P J F and Iijima S 2009 *Phys. Rev. Lett.* **102** 015501
[14] Roy H V, Kallinger C and Sattler K 1998 *Surface Sci.* **407** 1–6
[15] Qi L, Mao Y and Li J 2012 *Nanoscale* **4** 5989–5997
[16] Margine E R, Kolmogorov A N, Stojkovic D, Sofo J O and Crespi V H 2007 *Phys. Rev. B* **76** 115436
[17] Briddon P R and Jones R 2000 *Phys. Status Solidi* B **217** 131–171
[18] Goss J P, Shaw M J and Briddon P R 2007 *Theory of defects in semiconductors* (*Topics Appl. Phys.* vol 104) ed Drabold D A and Estreicher S K (Berlin Heidelberg: Springer-Verlag) chap 3, pp 69–94
[19] Rayson M J and Briddon P R 2008 *Computer Phys. Commun.* **178** 128–134
[20] Rayson M J 2007 *Phys. Rev.* E **76** 026704
[21] Perdew J P and Wang Y 1992 *Phys. Rev.* B **45** 13244–13249
[22] Perdew J P, Burke K and Ernzerhof M 1996 *Phys. Rev. Lett.* **77** 3865–3868
[23] Hartwigsen C, Goedecker S and Hutter J 1998 *Phys. Rev.* B **58** 3641–3662
[24] Latham C D, McKenna A J, Trevethan T P, Heggie M I, Rayson M J and Briddon P R 2015 *J. Phys: Condens. Matter.* **27** 316301
[25] Monkhorst H J and Pack J D 1976 *Phys. Rev.* B **13** 5188–5192
[26] Methfessel M and Paxton A T 1989 *Phys. Rev.* B **40** 3616–3621
[27] Schabel M C and Martins J L 1992 *Phys. Rev.* B **46** 7185–7188
[28] Charlier J, Gonze X and Michenaud J 1994 *Carbon* **32** 289–299
[29] Charlier J, Gonze X and Michenaud J 1994 *Europhys. Lett.* **28** 403–408
[30] Coulson C A, Herraez M A, Leal M, Santos E and Senent S 1963 *Proc. R. Soc. Lond., Ser. A* **274** 461–479
[31] El-Barbary A A, Telling R H, Ewels C P, Heggie M I and Briddon P R 2003 *Phys. Rev.* B **68** 144107
[32] Robertson A W, Montanari B, He K, Allen C S, Wu Y A, Harrison N M, Kirkland A I and Warner J H 2013 *ACS Nano* **7** 4495–4502
[33] Wadey J D, Markevich A, Robertson A, Warner J, Kirkland A and Besley E 2016 *Chem. Phys. Lett.* **648** 161–165
[34] Kotakoski J, Krasheninnikov A V, Kaiser U and Meyer J C 2011 *Phys. Rev. Lett.* **106** 105505
[35] Warner J H, Margine E R, Mukai M, Robertson A W, Giustino F and Kirkland A I 2012 *Science* **337** 209–212
[36] Lehtinen O, Kurasch S, Krasheninnikov A V and Kaiser U 2013 *Nature Commun.* **4**
[37] Tang Z, Hasegawa M, Shimamura T, Nagai Y, Chiba T, Kawazoe Y, Takenaka M, Kuramoto E and Iwata T 1999 *Phys. Rev. Lett.* **82** 2532–2535
[38] Shi C Q, Schut H and Li Z C 2016 *J. Phys.: Conf. Ser.* **674** 012019

[39] Suarez-Martinez I, Savini G, Haffenden G, Campanera J M and Heggie M I 2007 *Phys. Status Solidi* C **4** 2958–2962
[40] Jeong B W, Ihm J and Lee G-D 2008 *Phys. Rev. B* **78** 165403
[41] Suk M E and Aluru N R 2010 *J. Phys. Chem. Lett.* **1** 1590–1594
[42] Trevethan T, Latham C D, Heggie M I, Briddon P R and Rayson M J 2014 *Nanoscale* **6** 2978–2986
[43] Esquinazi P, Spemann D, Höhne R, Setzer A, Han K-H and Butz T 2003 *Phys. Rev. Lett.* **91** 227201
[44] Rode A V, Gamaly E G, Christy A G, Fitz Gerald J G, Hyde S T, Elliman R G, Luther-Davies B, Veinger A I, Androulakis J and Giapintzakis J 2004 *Phys. Rev. B* **70** 054407
[45] Faccio R and Mombrú A W 2012 *J. Phys: Condens. Matter.* **24** 375304
[46] Faccio R and Mombrú A W 2015 *Comp. Mater. Sci.* **97** 193–200
[47] Dai Q X, Zhao H J, Xie H M, Tang N Y, Li H Y and Zhao B 2011 *Euro. Phys. J. B* **80** 343–349
[48] Yazyev O V and Helm L 2007 *Phys. Rev. B* **75** 125408
[49] Ma Y, Lehtinen P O, Foster A S and Nieminen R M 2004 *New J. Phys.* **6** 68
[50] Yazyev O V 2010 *Rep. Prog. Phys.* **73** 056501
[51] Nelayev V V and Mironchik A I 2010 *Mater. Phys. Mech.* **9** 26
[52] Lieb E H 1989 *Phys. Rev. Lett.* **62** 1201–1204
[53] Banhart, F and Kotakoski, J and Krasheninnikov, A V *ACS Nano* **5** 26–41